Joint traveltime and waveform envelope inversion for near-surface imaging

Zhiyang Liu, Jie Zhang, University of Science and Technology of China (USTC)*

Summary

In the full waveform inversion, it is well known that a close initial model is needed when the ultra-low frequencies of data do not exist. Considering the problem, we propose a joint first-arrival traveltime and waveform envelope inversion method for the recovery of low-wavenumber model components to image near-surface structures. The envelopes of waveforms introduce low frequency data, and the traveltime inversion is a nonlinear and stable approach. The combination of the two approaches takes the advantages of both and also compensates the problems in each method. For example, the joint method is able to solve the hidden layer problem while traveltime inversion fails. Furthermore, the inverse matrix of traveltime sensitivity could serve as an effective preconditioner to the joint inversion. The result of our approach can be used as a reliable starting model for FWI, so that FWI can produce high-resolution results. We demonstrate the effectiveness of the joint inversion by applying to both synthetics and real data.

Introduction

Full waveform inversion (FWI) has gone through tremendous research and development efforts (Tarantola, 1984; Pratt, 1999). Although it has had impressive success in some cases (Sirgue et al., 2004), there exist many problems that need our attention. The first one is the lack of low frequencies in the data. Most of the energy of the updating gradient concentrates at the image interfaces. It is thus difficult to update the background model, if the data frequency is high. The second issue is the cycle skipping. When the initial model is far from the true one, the phase of the predicted or calculated data could be more than half a wavelength off. This generally leads to the convergence to a wrong model when using linear optimization procedures. This may also be caused by the lack of low frequencies in the data. We separate the two issues and propose a new solution with the current standard seismic data without low frequencies.

Wu et al. (2013) proposed a waveform envelope inversion method, which retrieves long-wavelength background velocity model without low-frequency source wavelet. This method extracts the ultra-low-frequency signals in seismic data to estimate a large scale of the model and the updating gradients. It boosts the low frequency component of the updating gradient and targets the updating of the background velocity model.

Zhang and Chen (2014) developed a joint traveltime and waveform inversion method for imaging the near-surface structure, which treats traveltime as a preconditioner for the near-surface inversion problem. It is a way to alleviate non-uniqueness of the model solutions and help speed up convergence significantly. If we maintain the traveltime consistency during the inversion, we can avoid the local minimum to some extent, i.e., reducing the cycle skipping problem.

In this study, we extract the low frequency component from data by accessing the envelopes of the waveforms for waveform inversion following Wu et al. (2013), and further combine that with the traveltime inversion. This leads to the development of a joint traveltime and waveform envelope inversion. We utilize the traveltime information to constrain the non-uniqueness of inversion and we use the waveform envelope information to obtain the background velocity for FWI. This approach can be used as an alternative method to produce a reliable starting model for FWI.

Gradient of waveform envelope data

First, we take a close look at what an inversion gradient looks like for a pair of source and receiver and how it is formed in depth. As we know, FWI gradient is a product of the source wave field and back propagated residual wave field from the receiver linked by the imaging condition. Theoretically, there are two different components in the gradient of reflection (Qin et al., 2013). One is the migration smile which contributes to the imaging energy of migration. The second is the one along the two segments of the reflection ray paths. It is the so called “rabbit ears”. This part is actually the low frequency noise that we try to remove in the reverse time migration when there are strong reflections caused by large velocity variations. Meanwhile, the gradient of early arrivals focuses its energy better on the component along raypath, but the energy is also lost on the “high-frequency smile”.

On the other hand, the gradient of waveform envelope data does not focus its energy on “high-frequency” smile component of either reflection or early arrivals, which shows its good property to retrieve long-wavelength structural information.

We extract the waveform envelope by taking the amplitude after analytic signal transform using the Hilbert transform. A signal having no negative-frequency components is called an analytic signal $\tilde{\mathbf{f}}(t)$, if it is constructed from a real signal $\mathbf{f}(t)$ and its transform $\mathbf{H}\{\mathbf{f}(t)\}$:

$$\tilde{\mathbf{f}}(t) = \mathbf{f}(t) + i\mathbf{H}\{\mathbf{f}(t)\} \quad (1)$$

The envelope $\mathbf{e}(t)$ of $\mathbf{f}(t)$ can be derived by:

$$\mathbf{e}(t) = \sqrt{\mathbf{f}^2(t) + \mathbf{H}^2\{\mathbf{f}(t)\}} \quad (2)$$

To compare FWI gradient with the gradient of waveform envelope data, we perform an impulse response test for a single seismic event of a single seismic trace. From Figure 1(a), we can observe that the rabbit ears of FWI are caused by reflection wave fields traveling along the same direction. And the migration smiles are produced by wave fields traveling at different directions. However, the gradient of waveform envelope data does not show significant migration smiles as shown in Figure 1(b). Similar phenomenon is also observed in the gradients of early arrivals, as shown in Figure 1(c) and Figure (d).

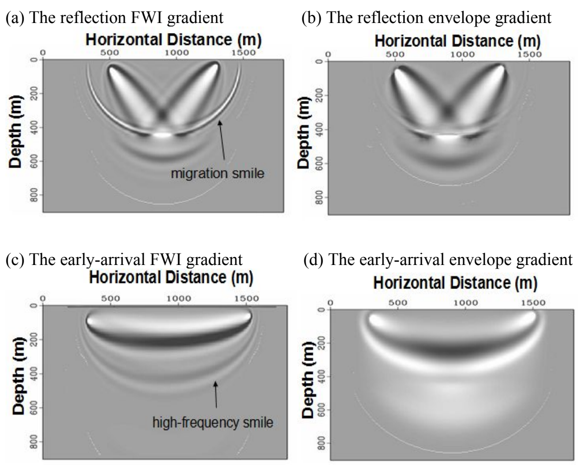

Figure 1: (a) The FWI gradient for reflection wave; (b) The envelope gradient for reflection wave; (c) The FWI gradient for early arrivals; (d) The envelope gradient for early arrivals;.

Therefore, to be able to update the ultra-low frequency background velocity model for FWI, we would like to extract and utilize the envelope information from seismic data.

Joint traveltime and waveform envelope inversion

In the following, we shall discuss the cycle skipping problem. When the starting model is far from the true one or the offset is large, the calculated and observed seismic traces may have too much phase differences that events match to the wrong ones. The effect is that each event pushes model updating to a different local minimum and the inversion fails to converge. However, if we utilize traveltime data to constrain model during waveform-based inversion, we can reduce the cycle skipping problem to some extent.

Combined with traveltime information, the objective function for joint traveltime and waveform envelope inversion can be imposed as follows:

$$\mathbf{\Phi(m)} = (1-w)\|\mathbf{e}_o - \mathbf{e}_c(\mathbf{m})\|^2 + w\|\mathbf{t}_o - \mathbf{t}_c(\mathbf{m})\|^2 + \alpha\|\mathbf{L}(\mathbf{m}-\mathbf{m}_0)\|^2 \quad (3)$$

where $\mathbf{e}_o$ is observed waveform envelope data, $\mathbf{e}_c$ is calculated waveform envelope data, $\mathbf{t}_o$ is picked traveltime, $\mathbf{t}_c$ is calculated traveltime, $\mathbf{m}$ is the velocity model, $\mathbf{m}_0$ is a priori model, **L** is a Laplacian operator for model regularization, and ω is a scaling factor between waveform envelope misfit and traveltime misfit.

Using Hilbert transform, equation (3) can be written as:

$$\begin{aligned}\mathbf{\Phi(m)} &= (1-w)\|(\mathbf{y}^2+\mathbf{y}_H^2)-(\mathbf{u}^2+\mathbf{u}_H^2)\| \\ &\quad + w\|\mathbf{t}_o - \mathbf{t}_c(\mathbf{m})\|^2 + \alpha\|\mathbf{L}(\mathbf{m}-\mathbf{m}_0)\|^2 \\ &= (1-w)\|\mathbf{E}\|^2 + w\|\mathbf{t}_o - \mathbf{t}_c(\mathbf{m})\|^2 + \alpha\|\mathbf{L}(\mathbf{m}-\mathbf{m}_0)\|^2\end{aligned} \quad (4a)$$

$$\mathbf{E} = (\mathbf{y}^2+\mathbf{y}_H^2)-(\mathbf{u}^2+\mathbf{u}_H^2) \quad (4b)$$

where **u** is the observed waveform, **y** is the calculated waveform, $\mathbf{u}_H$ and $\mathbf{y}_H$ are corresponding Hilbert transforms, and **E** is the instant envelope data residual.

We apply a nonlinear conjugate gradient method to minimize the above objective function, and calculate the following gradient that will determine the model update direction:

$$\frac{\partial\mathbf{\Phi(m)}}{\partial\mathbf{m}} = (1-w)\mathbf{F}^T\mathbf{P} - w\mathbf{A}^T(\mathbf{t}_o - \mathbf{t}_c(\mathbf{m})) + \alpha\mathbf{L}^T\mathbf{L}(\mathbf{m}-\mathbf{m}_0) \quad (5a)$$

$$\mathbf{F} = \frac{\partial\mathbf{y(m)}}{\partial\mathbf{m}} \quad (5b)$$

$$\mathbf{P} = \mathbf{E}^T\mathbf{y(m)} - \mathbf{H}\{\mathbf{E}^T\mathbf{y_H(m)}\} \quad (5c)$$

where **P** and **F** are the forward and backward propagation wavefields for envelope inversion that provides with sensitivity impact and directs model update, and **A** is a sensitivity matrix of traveltimes containing raypath information, equivalent to the impact of traveltime sensitivity. It should be noted that we can easily access **A** matrix after raytracing. Thus, we are able to invert for velocity model iteratively.

Applying this traveltime preconditioner should help finding the solutions to problem (3) quicker than by using the conventional gradient alone. The result can be used as the starting model for FWI, so that FWI can produce high-resolution results.

Synthetic tests

We apply our approach to a synthetic dataset generated from a model with a few velocity anomalies, as shown in Figure 2(a). The data are modeled assuming 100 shots with 50 m spacing and a Ricker wavelet with the peak frequency of 7 Hz. Also, the wavefield is recorded by 100 receivers with 50 m spacing. As described previously, we use the result of joint traveltime and waveform envelope inversion as the input model to FWI to help recover long-wavelength structure. Compared with FWI process, we can easily see the difference. The test results are shown in Figure 2. Figure 2 (c) depicts the result of the joint inversion which starts from a homogeneous model. Figure 2(d) shows the FWI solution after using the joint inversion result as an input model. The new procedure can recover correct velocity model without applying traveltime tomography before the joint inversion. Also, compared with the result from FWI procedure using traveltime tomography result as an initial model shown in Figure 2(e), our approach gives a better answer with fewer artifacts.

Furthermore, we apply our approach to a synthetic model with hidden layers which both traveltime inversion and FWI procedures often fail to converge. We set the true model as shown in Figure 3(a). The results are shown in Figure 3. As shown in Figure 3(b), velocity anomalies are not reconstructed by traveltime tomography. Also, Figure 3(e) shows that the FWI process using the traveltime tomography result as an initial model leads to a poor model solution. However, Figure 3(c) and (d) show better results, which may suggest the effectiveness of the new procedure. This is because the joint traveltime and waveform envelope inversion recovers long-wavelength background information and maintains the traveltime consistency simultaneously, as the iteration progresses. This eventually reduces artifacts and images the structures that traveltime tomography cannot. Also, it gives a more reasonable input for FWI than the traveltime tomography model.

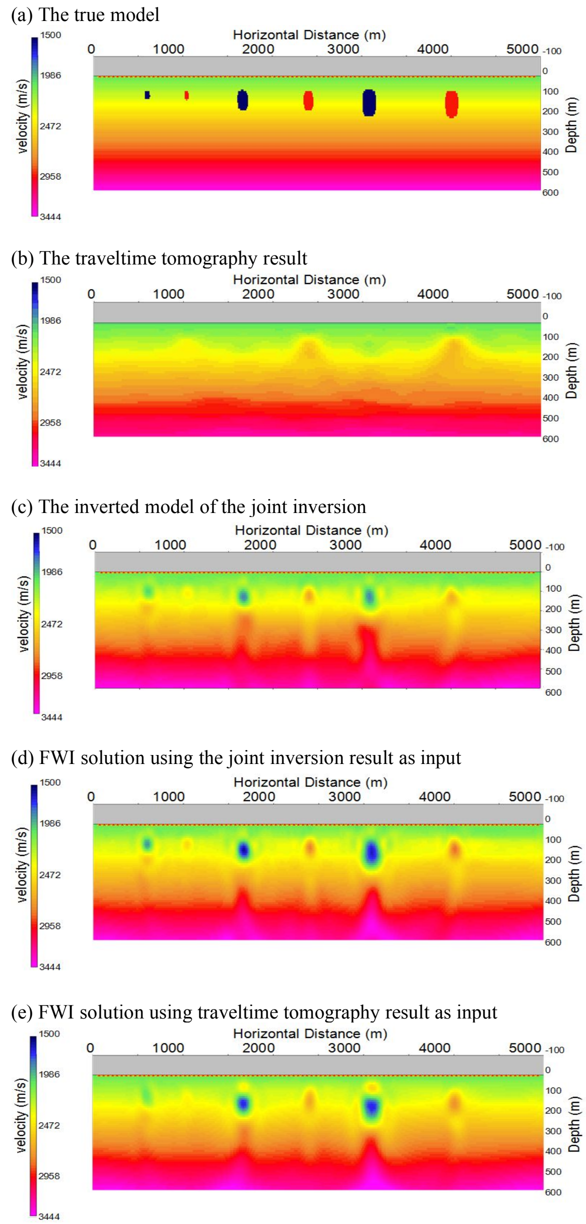

Figure 2: (a) The true model; (b) The traveltime tomography result; (c) The inverted model of joint traveltime and waveform envelope inversion; (d) The inverted model of FWI using the joint inversion result as an input model; (e) The inverted model of FWI using traveltime tomography result as an input model.

Joint Traveltime and Waveform Envelope Inversion

(a) The true model

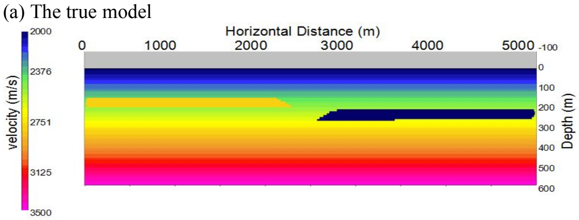

(b) The traveltime tomography result

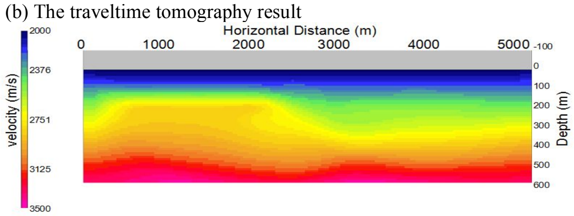

(c) The inverted model of the joint inversion

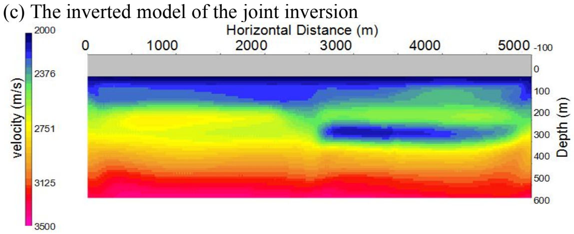

(d) FWI solution using the joint inversion result as input

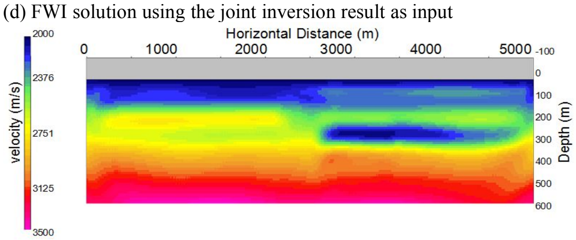

(e) FWI solution using traveltime tomography result as input

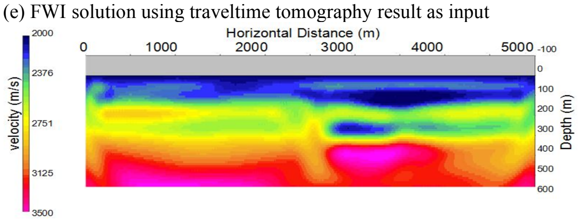

Figure 3: (a) The true model; (b) The traveltime tomography result; (c) The inverted model of joint traveltime and waveform envelope inversion; (d) The inverted model of FWI using the joint inversion result as an input model; (e) The inverted model of FWI using traveltime tomography result as an input model.

Field data applications

We apply the above method to field data on a 2D line. The survey is performed in an area where the topography is predominantly smooth. The data set includes 243 shots with 40 m spacing and 400 receivers with 20 m spacing.

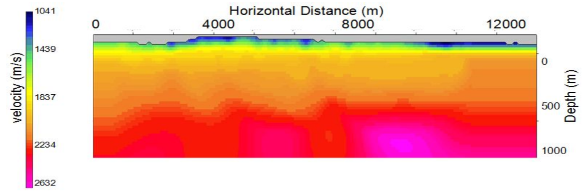

Figure 4: Traveltime tomographic solution using data on a 2D line.

(a) FWI solution using the joint inversion result as input

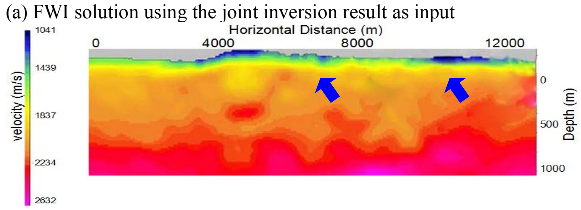

(b) FWI solution using traveltime tomography result as input

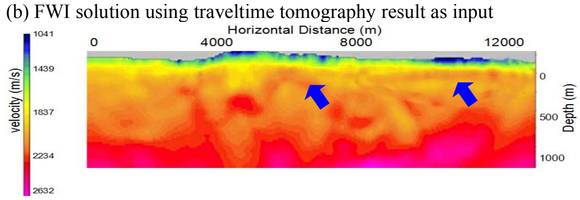

Figure 5: (a) The inverted model of FWI using the joint inversion result as an input model; (b) The inverted model of FWI using traveltime tomography result as an input model.

We normalize amplitudes and match the source spectrum to the field data during inversions. Figure 4 shows an initial model obtained by performing first-arrival traveltime tomography. Figure 5 shows the inversion results from this field data for both procedures. Overall, the relative deep model further varies, but the top near-surface area shows similar velocities to the traveltime tomography results. To be specific: in Figure 5 (b), the arrows indicate the areas where FWI solution departs from the traveltime tomographic solution and produces higher velocity. However, in Figure 5 (a), our procedure clearly brings that back.

Conclusions

We develop a joint traveltime and waveform envelope inversion for near-surface imaging. This approach is an effective algorithm to invert for long-wavelength structure in the near-surface area. It can help to build a fast converging FWI process for imaging the near-surface structure. The synthetic tests and application to field data further show the feasibility of the approach for solving an FWI problem.

Acknowledgments

We appreciate the support of GeoTomo, for allowing us to use the TomoPlus software package for this study.